An Extended Control of the Input Angle for Matrix Converters Connected with the Non-Unity Power Factor Loads.

Pawel Szczepankowski , *Member, IEEE*

***Abstract*—This paper proposes a novel PWM modulation algorithm for Multiphase Conventional Matrix Converters (MCMC), with 3 inputs and k outputs, using the transfer function of the load angle. The proposed approach extends the range of power angle control at the input during the operation with a maximum voltage transfer ratio. The proposed concept is based on the Direct Analytic Voltage PWM (DAV–PWM) modulation with an elliptical trajectory of reference load voltages. The proposal has been verified using the circuit simulation in PSIM software, symbolic analysis using Matlab, and finally through an experiment.**

***Index Terms*—matrix converters, AC/AC synthesis, pulse width modulation, input angle displacement control.**

NOMENCLATURE

j	Imaginary unit $\sqrt{-1}$.
t	Time.
T	Transposition of the matrix.
$\mathbf{v}_\mathrm{i}$	The analytic input voltages matrix.
$\mathbf{v}_\mathrm{ix}$	$=[v_{\mathrm{i1x}}, v_{\mathrm{i2x}}, v_{\mathrm{i3x}}]^T$ – the real parts of $\mathbf{v}_\mathrm{i}$.
$\mathbf{v}_\mathrm{iy}$	$=[v_{\mathrm{i1y}}, v_{\mathrm{i2y}}, v_{\mathrm{i3y}}]^T$ – the imaginary parts of $\mathbf{v}_\mathrm{i}$.
$\mathbf{v}_\mathrm{o}$	The analytic output reference voltages matrix.
k	Number of outputs.
$\mathbf{v}_\mathrm{ox}$	$=[v_{\mathrm{o1x}}, ..., v_{ok\mathrm{x}}]^T$ – the real parts of $\mathbf{v}_\mathrm{o}$.
$\mathbf{v}_\mathrm{oy}$	$=[v_{\mathrm{o1y}}, ..., v_{ok\mathrm{y}}]^T$ – the imaginary parts of $\mathbf{v}_\mathrm{o}$.
$\mathbf{i}_\mathrm{i}$	Averaged input currents $[i_{\mathrm{i1}}, i_{\mathrm{i2}}, i_{\mathrm{i3}}]^T$.
$\mathbf{i}_\mathrm{o}$	Measured output currents $[i_{\mathrm{o1}}, ..., i_{ok}]^T$.
$\mathbf{D}$	PWM duty cycle matrix with size $3 \times k$.
ϕ_i	Input displacement angle.
φ_o	Output displacement angle.
ω_i	$=2\pi f_\mathrm{i}$, where f_i is the input frequency.
ω_o	$=2\pi f_\mathrm{o}$, where f_o is the output frequency.
ψ_i	$=\omega_\mathrm{i} t$ the input voltage angle, $\psi_\mathrm{i} \in <0, 2\pi>$.
ψ_o	$=\omega_\mathrm{o} t$ the output voltage angle, $\psi_\mathrm{o} \in <0, 2\pi>$.
a, b	Semi–major, semi–minor axis of ellipse.
q	$=V_\mathrm{o}/V_\mathrm{i}$, voltage transfer ratio equal to a.
$\mathbf{\Gamma}$	Trajectory of reference voltages.
$\mathbf{\Pi}$	Voltage synthesis field.
T_PWM	Modulation period.
f_s	$=1/T_\mathrm{PWM}$ sampling frequency.

I. INTRODUCTION

THE Multiphase Conventional Matrix Converter (MCMC), shown in Fig. 1, is fed by a three–phase sinusoidal voltage source, which is connected to the load terminals using the true bidirectional semiconductor switches arranged into a $3 \times k$ matrix topology [1]–[3]. Such configuration can be divided into k cells with s_{1k}, s_{2k}, and s_{3k} switches. The single switch can be built from two transistors with two diodes or two RB–IGBT devices [1], [4], [5]. Each cell should be controlled to prevent line–to–line short circuits and to maintain a continuous load current flow [6], [7]. Comparing to AC/DC/AC back–to–back converters with large capacitors in DC–link, the matrix topology allows for direct AC–AC conversion using the small input filter, which is an advantage of these solutions. An important feature of the MCMC control is the possibility to adjust the input displacement angle ϕ_i shown in Fig. 2 [8]–[10].

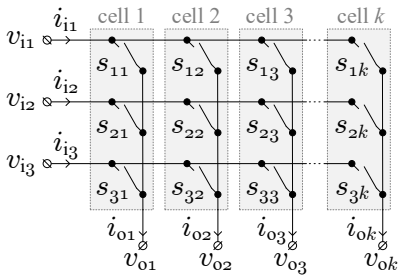

Fig. 1. The topology of the MCMC converter.

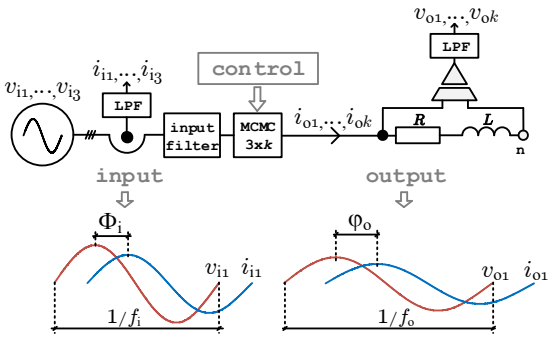

Fig. 2. General application scheme.

When MCs operate with the maximum voltage transfer ratio, it is not possible to change the input displacement angle using the standard modulation algorithms [1]. Hence, it is not possible to fully compensate for the offset introduced by the required input capacitive filter shown in Fig. 2. The zero value displacement angle may require a reduction in the voltage transfer ratio, which is disadvantageous. On the other

hand, reactive power generation may increase electricity bills. Matrix converters are very often used in the electric drive [1], [2]. However, the potential use of matrix converters is not only limited to these applications. This converter's type has been suggested to interconnect two independent power grids of different voltages and frequencies for the active and reactive power flow control between them [11]. The direct power control using Unified Power–Flow Controllers (UPFC) based on matrix converter, which does not have a large capacitors bank in the DC–link, could be an interesting alternative to classic solutions [12], [13]. The matrix converter can be also applied to compensate lagging power factor loads using inductors instead of electrolytic capacitors for energy storage. A concept of the capacitorless static synchronous compensator (STATCOM) with the model predictive control has been presented in [14]. Some papers deal with regulators and compensators for AC grids based on a hybrid transformer with a matrix converter realizing electrical coupling in that unit [15]–[17]. Extending the range of power angle control at the input of the MC increases the application potential in the area discussed above.

One can distinguish two general approaches to an input power factor control among the fundamental modulation methods. The first approach assumes that such a control is realised independently of the angle between the load voltage and current. In this case, only the stationary and zero vectors are involved in the switching sequence, and that concept of modulation is typical for direct, indirect and predictive methods based on the Space Vector Modulation (SVM) [1], [3]. If one neglects the shift generated by the applied input filter, which is shown in Fig. 2, the common relation between the input angle ϕ_{i} and the voltage gain q for topology $3 \times k$, can be written as follows

$$\phi_{\mathrm{i(SVM)}} = f(q,k) = \arccos(q/q_{\max}), \tag{1}$$

where $q_{\max}$ is the maximum voltage transfer ratio for the given system [18], [19]. For k equal to three and zero displacement angle, value of $q_{\max}$ is no greater than 0.866. However, the power factor less than the unity will decrease the voltage transfer ratio. The second fundamental approach to control the input displacement angle ϕ_{i} was proposed by Venturini and Alesina, and is based on the direct transfer functions [1], [3], [20], [21]. This solution allows for obtaining ϕ_{i} in the range

$$\phi_{\mathrm{i(VENTURINI)}} = g \cdot \varphi_{\mathrm{o}}, \tag{2}$$

where $g \in < -1, 1 >$. However, the drawback of this method is that the voltage transfer ratio cannot exceed 0.5. Moreover, the AC machine power factor varies according to the actual load condition and the range of φ_{o} is relatively tiny. Thus, the range of adjusting the input displacement angle ϕ_{i} is not effective for this type of application, and the superiority of SVM methods is indisputable here.

Extending the range of reactive power control in MC requires an analytical model. In three-phase systems, due to the symmetry of the system, such a model is proposed in two orthogonal references frame, for the input current and output voltage, respectively. Such reference frames contain a certain number of the selected vectors among the stationary, rotating and zero vector groups. Such a grouping is characteristic of the space-vector approach PWM modulation method. The relationship between the quantities at the input and output of the system can be represented by the fundamental transformation matrices. The PWM duty cycles are elements of these matrices and have to be finally calculated. Solving such a system of matrix equations requires the use of parametric dependencies or the use of linear programming algorithms. The implementation of such a general solution is not suitable for industrial implementation in real-time processors. Therefore, simplified solutions have been developed in the form of the direct and the indirect PWM algorithms [1]–[3].

Increasing the power angle control range can be realized by applying a mentioned general solution with computation effort. This methodology can be found in the work [22]. The disadvantage of this approach is the large number of systems of equations to be solved. If the number of outputs is greater than 5, the implementation of such an approach method becames quite complex in the practice because the total number of vectors involved by the Clarke transform is 3^k. An introduction of the known physical restriction of the conversion in CMC, such as limitation of the output voltage generation to the input voltage envelope, may reduce the modelling problem. A mathematical method for MC 3x3, which enhances the control range of input reactive power was presented in [23]. A lot of attention was paid to the description of mathematical constraints, a number of limitations were formulated. However, no explicit formulas for the PWM duty cycles for the proposed solution were finally given for the zero vectors. Similar considerations, also only for the 3x3 topology, are presented in [24]. The proposed solution is also based on the mathematical model. In comparison to the previous publication, the problem of the zero-sequence component and its constraints is explained. A complex analysis of the control extension, but for the sparse type MC, is presented in [25], but considerations do not cover the case of a larger number of output phases greater than three. A modulation technique for a 3x5 MC achieving a maximum input reactive power range, based on the load information, was proposed in [26]. However, implementation requires a proper setting of the free parameters in the optimisation formulas using complex formulas. With the increase of the number of output phases, the restrictions become more complex, and thus, the solution to the optimization problem is more difficult to obtain.

PWM modulation algorithms are developed using the space-vector approach and the Clarke transformation. For systems with fewer phases, this is the standard and effective approach, which also allows the input power angle control range to be extended. However, as research shows, as the number of phases increases, practical implementation of these solutions becomes very difficult. Thus, simpler way of presenting the problem and solving it is needed. Therefore, the goals of the considerations presented in the article are:

(A) reduction of the number of vectors needed to solve the problem,
(B) discussion of the influence of common–mode voltage on modulation properties,

(C) simplification and acceleration of the calculation of the PWM duty cycles,
(D) replacing a complex algebraic optimization with an equivalent graphical arrangement,
(E) and finally, proposing a truly universal solution for multiphase systems.

Points (A)–(C) are presented in section II and have a general form. Detailed descriptions of (D) and (E) are moved into section III. Results are presented and discussed in sections with simulation, experimental research, and conclusions.

II. The Concept of the General Solution

According to the concept proposed in [27], the input and reference voltages of MC3x3 can be represented by the Hilbert pairs, which consist of the real and the imaginary component, as shown in Fig. 3. These components are orthogonal to each other and can be represented by the set of the rotating vectors in xy plain. The set of input vectors moves in the Π_i plane, and the set of reference vectors moves in the Π_r plane. The angle

$$\sigma = \angle(\Pi_\mathrm{i}, \Pi_\mathrm{r}) \tag{3}$$

between these planes can be used to demonstrate the three main cases shown in in Fig. 4. The layout shown in Fig. 4(a) corresponds to the approach proposed by Venturini. Fig. 4(b) shows the graphical arrangement, which allows for developing the space–vector PWM methods [28]. Case (c) shows an intermediate solution that allows obtaining the maximum voltage transfer coefficient and a certain range of additional adjustment of the power angle at the input. The projection of the reference voltage trajectory Γ_r onto the xy plane (circle, line or an ellipse) does not have to fit inside the synthesis field. The collection of points, which correspond to the reference voltages, can be freely shifted inside the synthesis field and such an operation does not impact the generated line-to-line voltages. However, in general, adding the shift vector to the reference vectors changes the waveform of the common-mode voltage and number of switching. Considering the application of the elliptic trajectory, at least three shifting strategies can be briefly described.

The first layout, shown in Fig. 5(a) corresponds to the case, in which all reference points are located in the middle area of the triangular. The PWM duty cycles can be calculated using the simple rational functions for that arrangement, as follows

$$\mathbf{D}_{(\mathrm{a})} = \begin{bmatrix} d_{11} & d_{12} & d_{13} \\ d_{21} & d_{22} & d_{23} \\ d_{31} & d_{32} & d_{33} \end{bmatrix} = \frac{1}{\Delta_{123}} \begin{bmatrix} \Delta_{11} & \Delta_{12} & \Delta_{13} \\ \Delta_{21} & \Delta_{22} & \Delta_{23} \\ \Delta_{31} & \Delta_{32} & \Delta_{33} \end{bmatrix} \tag{4}$$

where symbol Δ corresponds to an appropriate a triangle' area depicted in Fig. 6, which can be calculated using the second–order determinant with x and y coordinates [29]. If the reference voltage does not slide along the edge of the triangle or stick to its vertex, then the waveforms of the PWM duty cycles are continuous. The total number of switching can be reduced by the connection of one of the reference points to one of the vertices of the synthesis field for some time. In

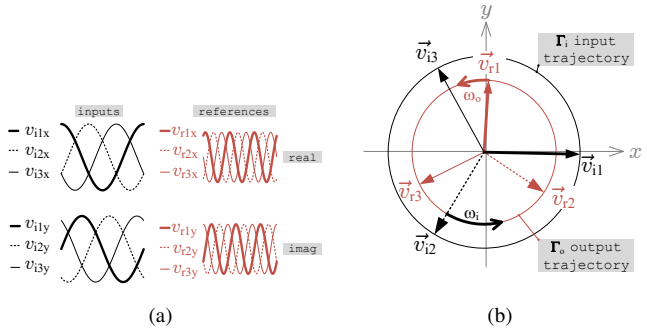

Fig. 3. The input and the reference voltages for MC3x3: (a) as the orthogonal pairs, (b) as the rotating vectors.

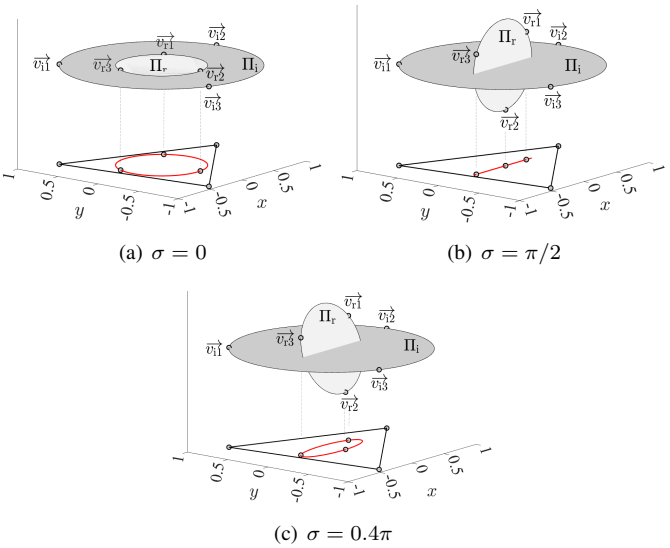

Fig. 4. Modification of the Π_r plane orientation.: (a) for Venturini method, (b) for space–vector PWM, (c) for the proposed approach.

such conditions, the matrix of the PWM duty cycles can be expressed as

$$\mathbf{D}_{(\mathrm{b})} = \begin{bmatrix} 1 & 0 & 0 \\ d_{21} & d_{22} & d_{23} \\ d_{31} & d_{32} & d_{33} \end{bmatrix} \tag{5}$$

Initial research found that the discontinuous modulation type II, depicted in Fig. 5(c), is the optimal approach because it allows for both, decreasing the number of switching, and simple shifting of an ellipse. The matrix of the PWM duty cycles can be rewritten as

$$\mathbf{D}_{(\mathrm{c})} = \begin{bmatrix} d_{11} & d_{12} & 0 \\ 0 & d_{22} & d_{23} \\ d_{31} & d_{32} & d_{33} \end{bmatrix} \tag{6}$$

The next section focuses on a detailed explanation of the chosen variant of the PWM modulation.

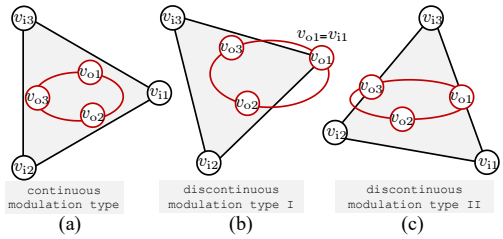

Fig. 5. Three variants of displacement way of reference points.

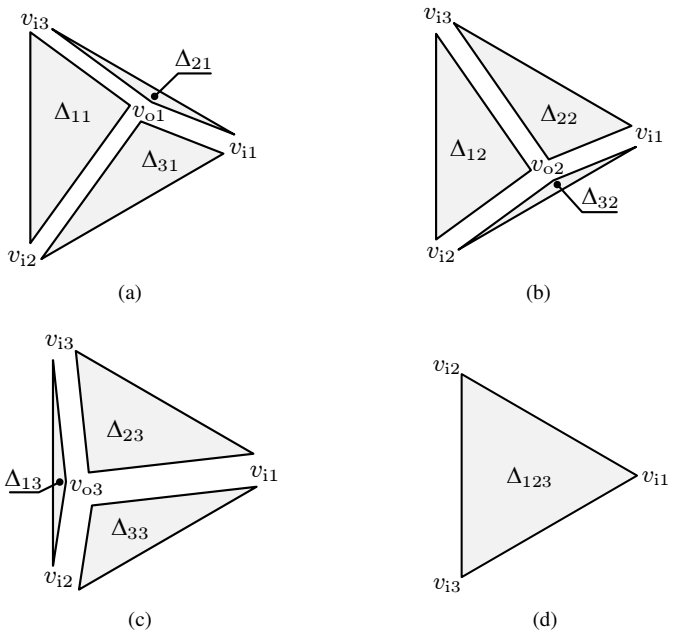

Fig. 6. An area of triangles as PWM duty cycles: (a) for the first load phase, (b) for the second load phase, (c) for the third load phase, (d) area of the synthesis field used as a normalisation factor in (4).

III. DAV-PWM MODULATION WITH AN ELLIPTICAL TRAJECTORY OF REFERENCE OUTPUT VOLTAGES

The proposed algorithm is implemented in 4 steps. In the first step, the input $\mathbf{v}_\mathrm{i}$

$$\mathbf{v_i} = V_\mathrm{i}\begin{bmatrix} \cos(\psi_\mathrm{i}) & \mathrm{j}\sin(\psi_\mathrm{i}) \\ \cos(\psi_\mathrm{i}-2\pi/3) & \mathrm{j}\sin(\psi_\mathrm{i}-2\pi/3) \\ \cos(\psi_\mathrm{i}+2\pi/3) & \mathrm{j}\sin(\psi_\mathrm{i}+2\pi/3) \end{bmatrix} \tag{7}$$

and reference load voltages $\mathbf{v}_\mathrm{r}$ are calculated

$$\mathbf{v_r} = V_\mathrm{i}\begin{bmatrix} a\cos(\psi_\mathrm{o}) & \mathrm{j}b\sin(\psi_\mathrm{o}) \\ a\cos(\psi_\mathrm{o}-\frac{2\pi}{3}) & \mathrm{j}b\sin(\psi_\mathrm{o}-\frac{2\pi}{3}) \\ a\cos(\psi_\mathrm{o}+\frac{2\pi}{3}) & \mathrm{j}b\sin(\psi_\mathrm{o}+\frac{2\pi}{3}) \end{bmatrix} \tag{8}$$

where $a \in < 0, q_{\max} >$ is a semi–major axis, b is a semi–minor axis of the ellipse. Next, two calculated ellipse offset coordinates $[v_\mathrm{sx}, v_\mathrm{sy}]$ are added to each point that represents the load reference voltage $\mathbf{v}_\mathrm{r}$

$$\mathbf{v_o} = V_\mathrm{i}\begin{bmatrix} a\cos(\psi_\mathrm{o})+v_\mathrm{sx} & \mathrm{j}(b\sin(\psi_\mathrm{o})+v_\mathrm{sy}) \\ a\cos(\psi_\mathrm{o}-\frac{2\pi}{3})+v_\mathrm{sx} & \mathrm{j}(b\sin(\psi_\mathrm{o}-\frac{2\pi}{3})+v_\mathrm{sy}) \\ a\cos(\psi_\mathrm{o}+\frac{2\pi}{3})+v_\mathrm{sx} & \mathrm{j}(b\sin(\psi_\mathrm{o}+\frac{2\pi}{3})+v_\mathrm{sy}) \end{bmatrix} \tag{9}$$

In the case of k–output converter, the output voltages $\mathbf{v}_\mathrm{o}$ can be expressed as

$$\mathbf{v_o}_{[\mathrm{kx2}]} = \mathbf{v_r}_{[\mathrm{kx2}]} + \begin{bmatrix} v_\mathrm{sx} & \mathrm{j}v_\mathrm{sy} \\ \dots & \dots \\ v_\mathrm{sx} & \mathrm{j}v_\mathrm{sy} \end{bmatrix}_{[\mathrm{kx2}]} \tag{10}$$

All required PWM duty cycles are calculated in step 4 using (4) for any reference points' positions. Note, that only the real part of the output voltage $\mathbf{v}_\mathrm{o}$ generates the voltage across the load. The imaginary part of this vector does not impact the average line–to-line output voltage. Any operation on the imaginary components is realised for the input displacement effect or obtaining a specific harmonic content in the input current. While the imaginary value for the output voltage in (9) can be given explicitly, the imaginary (orthogonal) part of the input voltage in (7) has to be computed. The grid voltages can be represented by rotating vectors with pulsation ω_i, which are shown in Fig. 3(b). In the case of the sinusoidal source, the real x and the imaginary y coordinates of these vectors can be calculated using various approaches using the Quadrature Filter, the Second Order Generalized Integrator structure or applying the Clark transform [28], [30]. The procedure of determining the shift vector plays a key role in the proposed modulation. The next subsection clarifies a basic idea of the shift–vector computation.

A. Calculation of the shift–vector coordinates

There are two proposals in this subsection. The first one is addressed to the case, in which the number of outputs is less than 8. For the remaining cases, a slightly different approach is proposed in the second subsection's part. The difference is that in the first case, the operation leads to a shift of the collection of the reference points (voltages) towards the inside of the synthesis field, while in the second solution, the entire trajectory should be shifted.

I. Solution of the shift–vector calculation for $k < 11$

Adding the shift–vector is required for an appropriate displacement of the reference points in the synthesis field. These points move on an elliptical trajectory, thus it is enough to find two characteristic points and move them so that they will be exactly on the edge of the triangular synthesis field - this corresponds to the case illustrated in Fig. 5(c). A single point, which is moving along the ellipse becomes the *characteristic point* if its distance from the edge of the triangle is the greatest – if the point lies outside the synthesis field, or the value is smallest – if the point resides inside. A distance criterion, expressed by the following formula

$$\Lambda \underset{p}{[g,h]} \underset{\cdots\cdots}{\overset{p \in \langle 1,k \rangle}{\cdots\cdots}} \det\left(\begin{bmatrix} v_{\mathrm{i}gx} & v_{\mathrm{i}gy} & 1 \\ v_{\mathrm{i}hx} & v_{\mathrm{i}hy} & 1 \\ v_{\mathrm{r}px} & v_{\mathrm{r}py} & 1 \end{bmatrix}\right) \tag{11}$$

should be calculated for each reference point and two selected lines given in the slope–intercept form $y = mx+n$. A variable g is the index of the first input voltage, while h corresponds to the second input voltage, and both voltages lie on the same line, which is one of the triangle edges. Considering the case

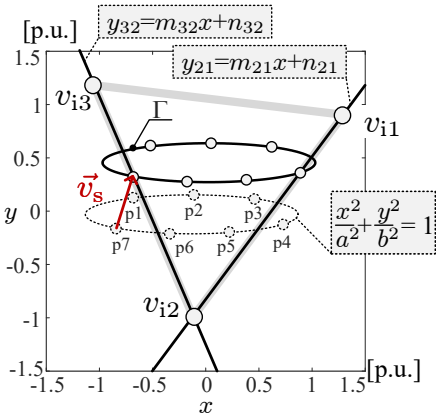

Fig. 7. A concept of Γ displacement using the shift–vector in the xy plane for $k < 11$.

shown in Fig. 7, which correspond to the CMC3x7 converter, two sets of the distance criterion can be proposed

$$\begin{aligned}\Lambda^{[3,2]} &= \min\left\{\Lambda^{[3,2]}_{1}, \Lambda^{[3,2]}_{2}, \ldots, \Lambda^{[3,2]}_{7}\right\}\\ \Lambda^{[2,1]} &= \min\left\{\Lambda^{[2,1]}_{1}, \Lambda^{[2,1]}_{2}, \ldots, \Lambda^{[2,1]}_{7}\right\}\end{aligned} \tag{12}$$

The indices of the two characteristic points are equal to the indices of the two minimal elements from (12),

$$\Lambda^{[3,2]} \equiv \Lambda^{[3,2]}_{7} \text{ and } \Lambda^{[2,1]} \equiv \Lambda^{[2,1]}_{4} \tag{13}$$

hence, the search values are 7 and 4. Now it's enough to solve the following system of equations

$$\begin{cases} v_{r7y} + v_{sy} = m_{32}\cdot(v_{r7x} + v_{sx}) + n_{32}\\ v_{r4y} + v_{sy} = m_{21}\cdot(v_{r4x} + v_{sx}) + n_{21}\end{cases} \tag{14}$$

with conditions

$$\{m_{32}, n_{32}\} = \begin{cases}\{\frac{v_{i23y}}{v_{i23x}}, v_{i2y} - m_{32}\cdot v_{i2x}\} & \Leftrightarrow \quad |v_{i23x}| > 0\\ \{0, v_{i2y}\} & \Leftrightarrow \quad v_{i23x} = 0\end{cases} \tag{15}$$

$$\{m_{21}, n_{21}\} = \begin{cases}\{\frac{v_{i21y}}{v_{i21x}}, v_{i2y} - m_{21}\cdot v_{i2x}\} & \Leftrightarrow \quad |v_{i21x}| > 0\\ \{0, v_{i2y}\} & \Leftrightarrow \quad v_{i21x} = 0\end{cases} \tag{16}$$

where v_{sx} and v_{sy} are the unknowns in the equation (14) and can be found using the determinant method. The formulas for the shift-vector coordinates can be calculated finally based on the following equations

$$\begin{aligned}v_{sx} &= \frac{v_{r7y} - v_{r4y} - m_1\cdot v_{r7x} + m_2\cdot v_{r4x} - n_1 + n_2}{m_1 - m_2}\\ v_{sy} &= \frac{m_1\cdot(v_{r7x}+v_{sx}) + m_2\cdot(v_{r4x}+v_{sx}) + n_1 + n_2 - v_{r7y} - v_{r4y}}{2}\end{aligned} \tag{17}$$

The calculations for the other two cases are analogous. It can be noticed that the calculation complexity of the shift–vector coordinates is the same for any number of the converter's output.

II. Solution of the shift–vector calculation for $k \geq 11$

For a large number of outputs - greater than 7 - the maximum voltage transfer ratio is near 0.75. In this case, only the

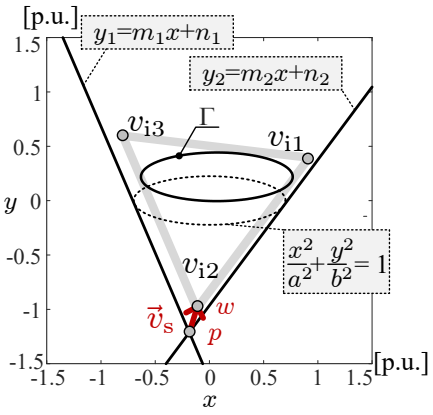

Fig. 8. A concept of Γ displacement using the shift–vector in the xy plane for $k \geq 11$.

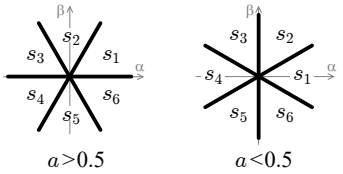

Fig. 9. Input voltage sectors.

trajectory Γ depicted in Fig. 8, is shifted, and no matter how many reference voltages move on it. The shift–vector $\vec{v}_s = \overrightarrow{wp}$ is calculated using coordinates of points p and w

$$\begin{aligned}v_{sx} &= w_x - p_x\\ v_{sy} &= w_y - p_y\end{aligned} \tag{18}$$

where

$$\begin{aligned}p_x &= \frac{n_2 - n_1}{m_1 - m_2}\\ p_y &= \frac{m_1\cdot n_2 - m_2\cdot n_1}{m_1 - m_2}\end{aligned} \tag{19}$$

The point w is the triangle vertex, which is the nearest to the intersection point p of two non–vertical straight lines, y_1 and y_2, parallel to the line–line voltage vectors. These two auxiliary straight lines are tangent to the master ellipse marked by the dotted line. Table I presents the final solution, which has been elaborated for each of the six input voltage sectors, shown in Fig. 9.

B. The range of a and b parameters.

The range of a parameter depends on an odd number of converter's outputs k, while the range of b parameter is a function of a

$$a_k \in \left\langle 0, \frac{1+\cos\left(\frac{\pi}{3}\right)}{2\cdot\cos\left(\frac{\pi}{2\cdot k}\right)}\right\rangle \quad b_k \in \langle 0, b_{k\,\max})\rangle \tag{20}$$

and $b_{k\,\max}$ can be calculated as follows

$$b_{k\,\max} = a_{k\,\max}\cdot\frac{\cos(\frac{\pi(k-1)}{k}) - 1}{\sqrt{3}\sin(\frac{\pi(k-1)}{k})} + \frac{\sqrt{3}}{2\sin(\frac{\pi(k-1)}{k})} \tag{21}$$

The maximum value of the $b_{k\,\max}$ parameter for the given value of k is shown in Table II. The maximum value of b_k, within the linear modulation range, can be determined

TABLE I
DATA NEEDED TO COMPUTE THE SHIFT–VECTOR IN EACH INPUT VOLTAGE SECTOR FOR $k > 7$.

for $a > 0.5$					
s_i	w	m_1	n_1	m_2	n_2
s_1	$v_{\mathrm{i}2}$	$\frac{v_{\mathrm{i}23\mathrm{y}}}{v_{\mathrm{i}23\mathrm{x}}}$	$-\xi_1$	$\frac{v_{\mathrm{i}21\mathrm{y}}}{v_{\mathrm{i}21\mathrm{x}}}$	$-\xi_2$
s_2	$v_{\mathrm{i}1}$	$\frac{v_{\mathrm{i}12\mathrm{y}}}{v_{\mathrm{i}12\mathrm{x}}}$	ξ_1	$\frac{v_{\mathrm{i}13\mathrm{y}}}{v_{\mathrm{i}13\mathrm{x}}}$	ξ_2
s_3	$v_{\mathrm{i}3}$	$\frac{v_{\mathrm{i}32\mathrm{y}}}{v_{\mathrm{i}32\mathrm{x}}}$	$-\xi_1$	$\frac{v_{\mathrm{i}31\mathrm{y}}}{v_{\mathrm{i}31\mathrm{x}}}$	$-\xi_2$
s_4	$v_{\mathrm{i}2}$	$\frac{v_{\mathrm{i}23\mathrm{y}}}{v_{\mathrm{i}23\mathrm{x}}}$	ξ_1	$\frac{v_{\mathrm{i}21\mathrm{y}}}{v_{\mathrm{i}21\mathrm{x}}}$	ξ_2
s_5	$v_{\mathrm{i}1}$	$\frac{v_{\mathrm{i}12\mathrm{y}}}{v_{\mathrm{i}12\mathrm{x}}}$	$-\xi_1$	$\frac{v_{\mathrm{i}13\mathrm{y}}}{v_{\mathrm{i}13\mathrm{x}}}$	$-\xi_2$
s_6	$v_{\mathrm{i}3}$	$\frac{v_{\mathrm{i}32\mathrm{y}}}{v_{\mathrm{i}32\mathrm{x}}}$	ξ_1	$\frac{v_{\mathrm{i}31\mathrm{y}}}{v_{\mathrm{i}31\mathrm{x}}}$	ξ_2
for $a < 0.5$					
s_i	w	m_1	n_1	m_2	n_2
s_1	$v_{\mathrm{i}1}$	$\frac{v_{\mathrm{i}13\mathrm{y}}}{v_{\mathrm{i}13\mathrm{x}}}$	ξ_1	$\frac{v_{\mathrm{i}12\mathrm{y}}}{v_{\mathrm{i}12\mathrm{x}}}$	$-\xi_2$
s_2	$v_{\mathrm{i}3}$	$\frac{v_{\mathrm{i}31\mathrm{y}}}{v_{\mathrm{i}31\mathrm{x}}}$	ξ_1	$\frac{v_{\mathrm{i}32\mathrm{y}}}{v_{\mathrm{i}32\mathrm{x}}}$	$-\xi_2$
s_3	$v_{\mathrm{i}2}$	$\frac{v_{\mathrm{i}21\mathrm{y}}}{v_{\mathrm{i}21\mathrm{x}}}$	ξ_1	$\frac{v_{\mathrm{i}23\mathrm{y}}}{v_{\mathrm{i}23\mathrm{x}}}$	$-\xi_2$
s_4	$v_{\mathrm{i}1}$	$\frac{v_{\mathrm{i}13\mathrm{y}}}{v_{\mathrm{i}13\mathrm{x}}}$	$-\xi_1$	$\frac{v_{\mathrm{i}12\mathrm{y}}}{v_{\mathrm{i}12\mathrm{x}}}$	ξ_2
s_5	$v_{\mathrm{i}3}$	$\frac{v_{\mathrm{i}31\mathrm{y}}}{v_{\mathrm{i}31\mathrm{x}}}$	$-\xi_1$	$\frac{v_{\mathrm{i}32\mathrm{y}}}{v_{\mathrm{i}32\mathrm{x}}}$	ξ_2
s_6	$v_{\mathrm{i}2}$	$\frac{v_{\mathrm{i}21\mathrm{y}}}{v_{\mathrm{i}21\mathrm{x}}}$	$-\xi_1$	$\frac{v_{\mathrm{i}23\mathrm{y}}}{v_{\mathrm{i}23\mathrm{x}}}$	ξ_2
where $\xi_1 = \sqrt{{b_{\max}}^2 + (am_1)^2}$ and $\xi_2 = \sqrt{{b_{\max}}^2 + (am_2)^2}$					

TABLE II
THE MAXIMUM VALUE OF THE $b_{k\,\max}$ PARAMETER.

k	$a_{\max}$	$b_{\max}$
3	0.866	0.134
5	0.788	0.072
7	0.769	0.051
11	0.757	0.031
13	0.755	0.026

by the analysis of characteristic positions of an ellipse and its intersecting points with the edges of the synthesis field. Assuming the maximum semi–major axis a of an ellipses Γ_o shown in Fig. 10(a)–(b), it is apparent that at least three of these points belong both, to an ellipse, and the synthesis field. For $k \geq 11$ another general solution can be proposed. There are two general cases for consideration. In the first case, shown in Fig. 10(c), the semi–major axis a is greater than the semi–minor axis $b_{\max}$ of the ellipse defined by the following parametric formula

$$\begin{aligned} x_\Gamma &= a \cdot \cos(\psi_\mathrm{o}) + a - 0.5 \\ y_\Gamma &= b_{\max} \cdot \sin(\psi_\mathrm{o}) \end{aligned} \tag{22}$$

where

$$\begin{aligned} b_{\max} &= f(a) \overset{a>0.5}{=} \sqrt{n^2 - a^2 \cdot m^2} \\ m &\overset{\psi_\mathrm{i}=0}{=} \frac{v_{\mathrm{i}3\mathrm{y}} - v_{\mathrm{i}1\mathrm{y}}}{v_{\mathrm{i}3\mathrm{x}} - v_{\mathrm{i}1\mathrm{x}}} \\ n &\overset{\psi_\mathrm{i}=0}{=} v_{\mathrm{i}3\mathrm{y}} - m \cdot v_{\mathrm{i}3\mathrm{x}} + m \cdot (a - 0.5) \end{aligned} \tag{23}$$

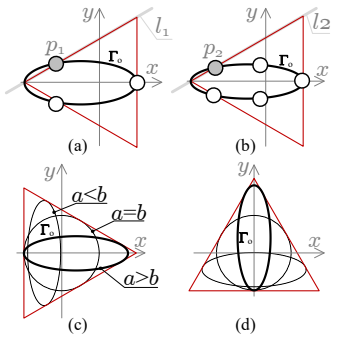

Fig. 10. Characteristic positions of the ellipse Γ inside the synthesis field: (a) for CMC3x3, (b) for CMC3x5, (c) and (d) for CMC3xk and $k \geq 11$.

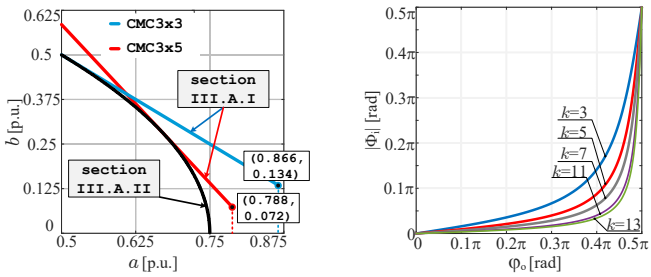

(a) $b = f(a)$ (b) $\phi_\mathrm{i} = f(\varphi_\mathrm{o}, a_{k\,\max})$

Fig. 11. Applicability range: (a) of an ellipse parameters, (b) of an input displacement angle control for maximum voltage transfer ratio.

For $a = 0.75$ the semi–minor axis b is zero. When $a < 0.5$ the maximum value of the semi–minor axis can be elaborated using a graphical arrangement depicted in Fig. 10(d). The parametric form of an ellipse can be expressed as

$$\begin{aligned} x_\Gamma &= a \cdot \cos(\psi_\mathrm{o}) \\ y_\Gamma &= b_{\max} \cdot \sin(\psi_\mathrm{o}) + b - 0.5 \end{aligned} \tag{24}$$

where

$$\begin{aligned} b_{\max} &= f(a) \overset{a<0.5}{=} \frac{n^2 + n + 0.25 - (m \cdot a)^2}{(2 \cdot n + 1)} \\ m &\overset{\psi_\mathrm{i}=-\pi/6}{=} \frac{v_{\mathrm{i}3\mathrm{y}} - v_{\mathrm{i}1\mathrm{y}}}{v_{\mathrm{i}3\mathrm{x}} - v_{\mathrm{i}1\mathrm{x}}} \\ n &\overset{\psi_\mathrm{i}=-\pi/6}{=} 1 \end{aligned} \tag{25}$$

The proposed second modulation variant, for $k \geq 11$, does not allow for a non–zero setting of the input displacement angle at the input of the system when MC operates with the maximum voltage transfer ratio. A theoretical applicability range of the proposed modulation is presented in Fig. 11.

C. The control of an input power factor

For a given output displacement angle φ_o and the load current amplitude $I_{\max}$, the input currents in $\alpha\beta$ plane can be analytically expressed as

$$\begin{aligned} i_{\mathrm{i}\alpha}(\psi_\mathrm{i}) &= I_{\max} \cdot (a \cdot \cos(\varphi_\mathrm{o}) \cdot \cos(\psi_\mathrm{i}) - b \cdot \sin(\varphi_\mathrm{o}) \cdot \sin(\psi_\mathrm{i})) \\ i_{\mathrm{i}\beta}(\psi_\mathrm{i}) &= I_{\max} \cdot (a \cdot \cos(\varphi_\mathrm{o}) \cdot \sin(\psi_\mathrm{i}) + b \cdot \sin(\varphi_\mathrm{o}) \cdot \cos(\psi_\mathrm{i})) \end{aligned} \tag{26}$$

Equations (26) can be transformed to the form, in which the current's vector $[i_{\mathrm{i}\alpha}(\psi_\mathrm{i} = 0), i_{\mathrm{i}\beta}(\psi_\mathrm{i} = 0)]$ with a constant start position is multiplied by the rotation matrix $\mathbf{R}$ as follows

$$[i_{\mathrm{i}\alpha}(\psi_\mathrm{i}), i_{\mathrm{i}\beta}(\psi_\mathrm{i})] = I_{\max} \cdot [a \cdot \cos(\varphi_\mathrm{o}), b \cdot \sin(\varphi_\mathrm{o})] \cdot \mathbf{R} \tag{27}$$

where

$$\mathbf{R} = \begin{bmatrix} \cos(\psi_\mathrm{i}) & -\sin(\psi_\mathrm{i}) \\ \sin(\psi_\mathrm{i}) & \cos(\psi_\mathrm{i}) \end{bmatrix} \tag{28}$$

Thus, the tangent of the input displacement angle can be derived directly from (27)

$$\tan(\phi_\mathrm{i}) = \frac{b}{a} \cdot \tan(\varphi_\mathrm{o}) \tag{29}$$

The comparison of two DAV–PWM algorithms with the straight–line (denote by subscript L) and the elliptic (denote by subscript E) trajectory is presented in Table III.

TABLE III
THE COMPARISON OF DAV–PWM$_\mathrm{L}$ AND DAV–PWM$_\mathrm{E}$.

	DAV–PWM$_\mathrm{L}$ or SVM	DAV–PWM$_\mathrm{E}$
$\frac{v_{\mathrm{i}1\mathrm{x}}}{V_\mathrm{i}}$	$\cos(\psi_\mathrm{i})\cos(\phi_\mathrm{i}) - \sin(\psi_\mathrm{i})\sin(\phi_\mathrm{i})$	$\cos(\psi_\mathrm{i})$
$\frac{v_{\mathrm{i}1\mathrm{y}}}{V_\mathrm{i}}$	$\cos(\psi_\mathrm{i})\sin(\phi_\mathrm{i}) + \sin(\psi_\mathrm{i})\cos(\phi_\mathrm{i})$	$\sin(\psi_\mathrm{i})$
$\frac{v_{\mathrm{o}1\mathrm{x}}}{V_\mathrm{i}}$	$q\cos(\psi_\mathrm{o}) + v_{\mathrm{sx}}$	$a\cos(\psi_\mathrm{o}) + v_{\mathrm{sx}}$
$\frac{v_{\mathrm{o}1\mathrm{y}}}{V_\mathrm{i}}$	v_{sy}	$b\sin(\psi_\mathrm{o}) + v_{\mathrm{sy}}$
$q_{\max}$	$q_{3\,\max} = 0.866$ $q_{11\,\max} = 0.75$	see Table II
$\frac{i_{\mathrm{i}\alpha}}{I_{\max}}$	$q\cos(\varphi_\mathrm{o})\cos(\phi_\mathrm{i} + \psi_\mathrm{i})$	$a\cos(\varphi_\mathrm{o})\cos(\psi_\mathrm{i}) - b\sin(\varphi_\mathrm{o})\sin(\psi_\mathrm{i})$
$\frac{i_{\mathrm{i}\beta}}{I_{\max}}$	$q\cos(\varphi_\mathrm{o})\sin(\phi_\mathrm{i} + \psi_\mathrm{i})$	$a\cos(\varphi_\mathrm{o})\sin(\psi_\mathrm{i}) + b\sin(\varphi_\mathrm{o})\cos(\psi_\mathrm{i})$
ϕ_i control	direct	indirect by (29)
PWM method	discontinuous	discontinuous - section A.I, continuous - section A.II

The comparison of the DAV–PWM$_\mathrm{L}$ with Venturini and Extended Venturini method has been done in paper [27]. The next comparison of this algorithm with the SVM method has been performed in work [30]. As can be deduced, the control of the input displacement angle in the case of DAV–PWM$_\mathrm{L}$ is direct and depends on the angular shift of the input voltage vectors. However, the DAV–PWM$_\mathrm{E}$ method of modulation allows for transferring the output displacement angle to the input. The comparison of an input displacement control range for these modulation methods is presented in Fig. 12. The simplified diagram of the proposed DAV–PWM$_\mathrm{E}$ modulation is presented in Fig. 13. The green colour accentuates the change in the case of the number of outputs greater than 3.

IV. RESULTS

The research was performed in two stages. The proposed algorithm for the number of outputs greater than 3 was verified at the first stage using the converters topology 3x5 and 3x11. The simulation scheme included only the elementary elements, such as the AC voltage sources, the matrix converter, and resistance–inductive load. The aim of the research in the second stage was to demonstrate the convergence of the simulation and experimental results for $k = 3$, assuming that the MC operates with the maximum voltage transfer ratio of $a_{3\,\max} = q_{\max} = 0.86$. The values of supply voltages and

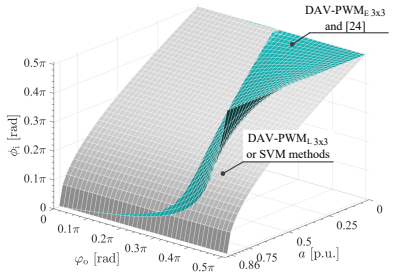

(a) CMC3x3 – modulation variant from section III.A.I

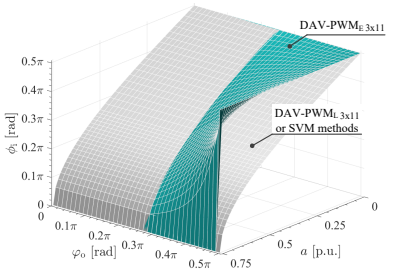

(b) CMC3x11 – modulation variant from section III.A.II

Fig. 12. The theoretical range of an input displacement angle as a function of the load angle φ_o and the voltage transfer ratio a for two types of the DAV–PWM modulations.

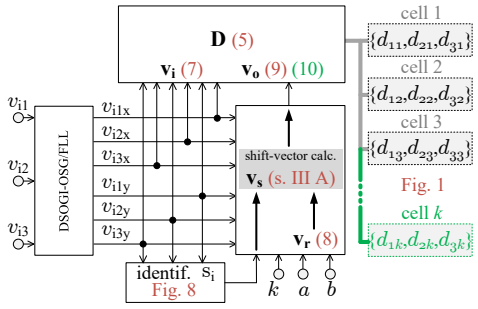

Fig. 13. Simplified modulation DAV–PWM$_\mathrm{E}$ diagram.

load parameters were appropriately selected for obtaining a measurable effect of transferring the load angle to the 5kVA converter's input. The research, therefore, did not cover a specific application but contributed to the demonstration of the PWM modulation capabilities. The simulation parameters are shown in Table IV. The parameters set for the experiment have been the same as the simulation parameters for $k = 3$. Algorithms were supported by the DLL library with user C–code. The schematic diagram for a simulation and experiment using CMC3x3 converter is presented in Fig. 14. Photos of the hardware configurations are shown in Fig. 15 for testing the 3×3 topology, and in Fig. 16 for $3\times k$ topologies, respectively.

A. Simulations for $k = 5$ and $k = 11$

Simulation results for $k = 5$ and maximum $a = 0.788$ for three example values of b parameter are presented in Fig. 17(a). In contrast to the proposed modulation algorithm, for such a value of voltage transfer ratio a both methods, SVM

TABLE IV
THE SIMULATION PARAMETERS.

name	value
software	PSIM11
T_{PWM}	for 100μs
step	10ns
the load resistance R for $k = 5; 11$	0.1Ω
the load resistance R for $k = 3$	1Ω
the load inductance L for $k = 3; 5; 11$	6mH
the input line–to–line voltage for $k = 5; 11$	3×100 $\mathrm{V_{AC}}$, 50Hz
the input line–to–line voltage for $k = 3$	$3 \times 50\sqrt{3}$ $\mathrm{V_{AC}}$, 50Hz
schematic for $k = 5; 11$	simplified RL, any filters
schematic for $k = 3$	as in Fig. 14 also at experiment

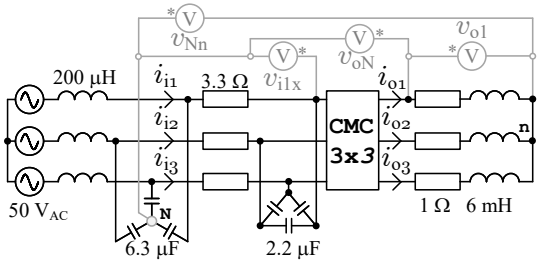

Fig. 14. The schematic diagram for a simulation and experiment using CMC3x3 converter.

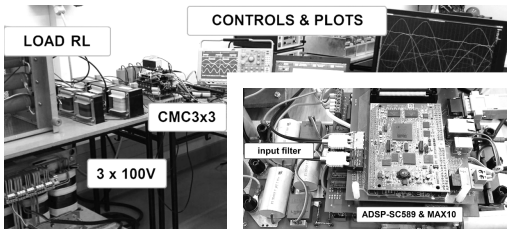

Fig. 15. Photo of the hardware configuration CMC3x3 in the laboratory.

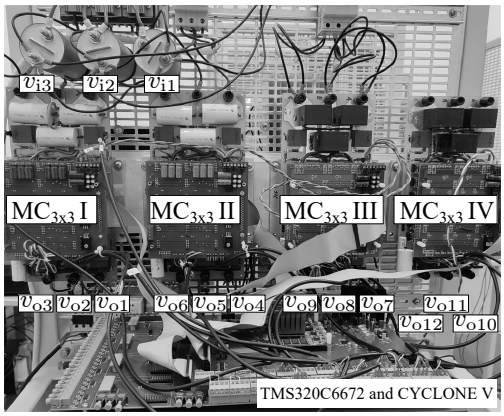

Fig. 16. Photo of the hardware configuration CMC3x12 in the laboratory.

and DAV–PWM$_{\mathrm{L}}$, are not able to generate nonzero input displacement angle due to their theoretical constraints. As can be seen, during the operation with a maximum q, one

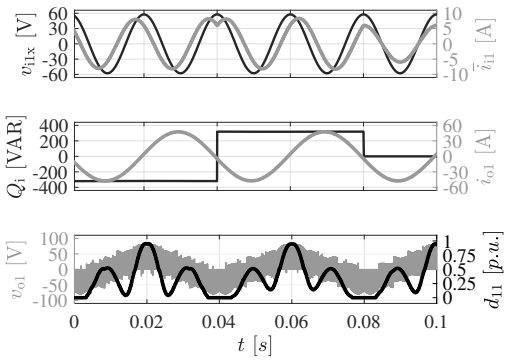

(a) $k = 5$, $\omega_{\mathrm{o}} = \omega_{\mathrm{i}}/2$, $a = 0.788$, $b = \{0.073, -0.073, 0\}$, $\phi_{\mathrm{i}}(b) = \{-0.22\pi, 0.22\pi, 0\}$

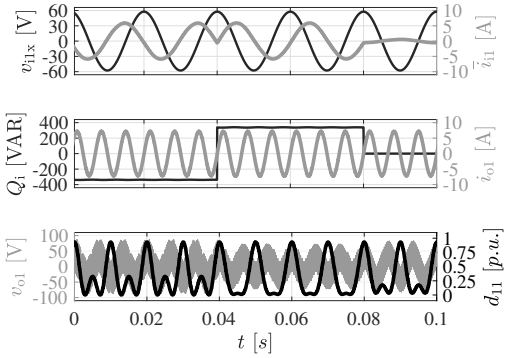

(b) $k = 11$, $\omega_{\mathrm{o}} = 3\omega_{\mathrm{i}}$, $a = 0.7$, $b = \{0.223, -0.223, 0\}$, $\phi_{\mathrm{i}}(b) = \{-0.48\pi, 0.48\pi, 0\}$

Fig. 17. The influence of the step change of parameter b on the input displacement angle and the reactive instantaneous power: (a) MCMC3x5, (b) MCMC3x11.

can obtain an input displacement angle of about 0.22π. If $k = 11$, the second solution of the shift–vector calculation can be applied. For that value of k, DAV–PWM$_{\mathrm{L}}$ and SVM modulations have the same limit of $q_{11\,\max} = 0.75$ and both algorithms do not allow to generate the reactive power at the converter's input. However, it can be shown that the transfer of the load angle (29) allows obtaining a greater input angle than SVM or DAV–PWM$_{\mathrm{L}}$ methods for the load parameters under the following condition

$$\left|\arccos\left(\frac{q_k}{q_{k\ \max}}\right)\right| < \left|\arctan\left(\frac{b \cdot \omega_{\mathrm{o}} L}{a \cdot R}\right)\right| \qquad (30)$$

Simulation results for $k = 11$ and maximum $a = 0.7$ for three example values of b parameter are presented in Fig. 17(b). Using (30) one obtains $0.1169\pi < 0.4824\pi$, which proves the advantage of the proposed concept.

B. Experimental results for $k = 3$ and $k = 5$

The results of a step change of parameter b to the input displacement angle and the generation of the input reactive power Q_{i} for $a = 0.86$ and $\omega_{\mathrm{o}} = 2$ are presented in Fig. 18(b). As can be seen in Fig. 18(c), the simulation and experimental results converge and show that the proposed solution allows for controlling the input power angle ϕ_{i} within a certain range under the maximum voltage transfer ratio $q = 0.86$.

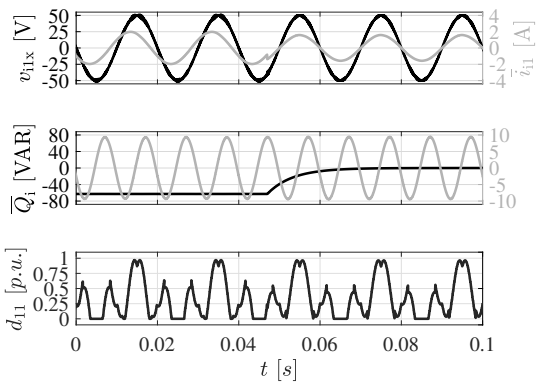

(a) simulation

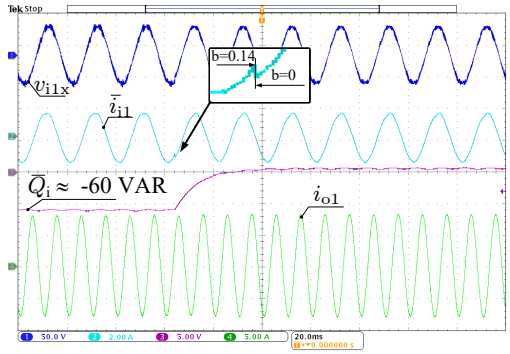

(b) experiment

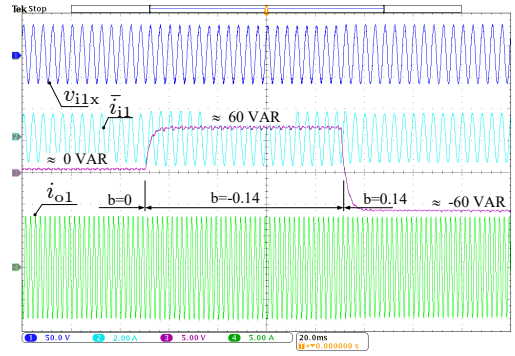

(c) experiment

Fig. 18. The result of a step change of parameter b to the generation of the input reactive power Q_i for $a = 0.86$, $\omega_o = 2\omega_i$, and $k = 3$.

The experimental result for CMC3 $\times$ 5 shown in Fig. 16 were performed for $R = 47\ \Omega$ and $L = 6$ mH with a maximum voltage transfer transfer ratio of 0.78. Load voltage waveforms and the change of reactive power at the input in the case of a step change of parameter b are shown. The greater the number of converter outputs limits the load angle transfer range to the input (29) under the maximum voltage transfer ratio (20), as can be illustrated in Fig. 11(b). The modification of the reference output voltage trajectory (the transition shown from an ellipse to the straight line) does not affect the generated average load currents when the a parameter remains unchanged.

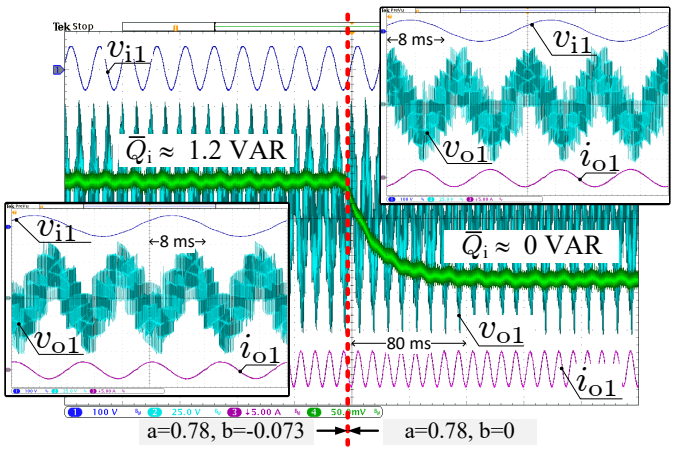

Fig. 19. The result of a step change of parameter b for $a = 0.78$, $\omega_o = 2\omega_i$, and $k = 5$.

V. Conclusion

Extended control of the input angle for multiphase conventional matrix converter connected with the non-unity power factor loads has been presented during operation under maximum voltage transfer ratio. The main advantages of the proposal are:

(A) The total number of required vectors is equal to $3+k$ and it's much less compared to the SVM method, in which the total number of the considered vectors is equal to 3^k (Fig.3, Fig. 4).

(B) The geometric arrangement consisting of an ellipse and a triangle allows one to easily see the conduction states and the blocking of power electronic connectors. The mechanism of shifting this ellipse allows obtaining the continuous or discontinuous type of the PWM modulation (Fig. 5).

(C) No complicated formulas are needed to calculate the values of the PWM duty cycles. Calculations are based on coordinates of the points shown in Fig. 6 and the formula for the area of the triangle. Such an approach frees the algorithm from the trigonometric form of the solution and speeds up the computation [30].

(D) As discussed in the introduction, the problem has been reduced to a geometric form, where all constraints are explicitly specified and no advanced parametric optimization is needed.

(E) The presented solution can be applied to any number of outputs. However, the trajectory shifting mechanism, which corresponds to the load angle transfer function, is limited by the increasing number of load outputs.

To compared to the SVM method, two disadvantages can be formulated. (1) The SVM methods for multiphase systems are considered in the multi–orthogonal space–vector frames, which can be used for example – (a) for torque increasing, (b) control of the two–speed mechanical system [31], [32]. The proposed solution operates only within the first orthogonal space. (2) The switches' states are not tabularized and optimized as in SVM algorithms. Thus, the proposed approach, which is based on the commutation cells shown in Fig. 1

does not cover this issue and the switching losses can be inestimable.

Finally, the same results were obtained as in [24]. With reference to [26], it can only be stated that the proposed method is simpler, the exact comparison requires further research. The proposal innovative rely on the applicability of the solution to a greater number of outputs than 5.

REFERENCES

[1] J. Rodriguez, M. Rivera, J. Kolar, and P. Wheeler, "A review of control and modulation methods for matrix converters," *IEEE Trans. Ind. Electron.*, vol. 59, DOI 10.1109/TIE.2011.2165310, no. 1, pp. 58–70, Jan. 2012.

[2] L. Helle, K. Larsen, A. Jorgensen, S. Munk-Nielsen, and F. Blaabjerg, "Evaluation of modulation schemes for three-phase to three-phase matrix converters," *IEEE Trans. Ind. Electron.*, vol. 51, DOI 10.1109/TIE.2003.821900, no. 1, pp. 158–171, Feb. 2004.

[3] T. Friedli and J. Kolar, "Milestones in matrix converter research," *IEEJ Journal of Industry Application*, vol. 1, DOI 10.1541/ieejjia.1.2, no. 1, pp. 2–14, Jul. 2012.

[4] S. Mori, M. Aketa, T. Sakaguchi, H. Asahara, T. Nakamura, and T. Kimoto, "Suppression of punch-through current in 3 kv 4h-sic reverse-blocking mosfet by using highly doped drift layer," *IEEE Journal of the Electron Devices Society*, vol. 6, DOI 10.1109/JEDS.2018.2819681, pp. 449–453, 2018.

[5] J. W. Kolar, T. Friedli, J. Rodriguez, and P. W. Wheeler, "Review of three-phase pwm ac-ac converter topologies," *IEEE Transactions on Industrial Electronics*, vol. 58, DOI 10.1109/TIE.2011.2159353, no. 11, pp. 4988–5006, 2011.

[6] S. Tammaruckwattana, Chenxin Yue, Y. Ikeda, and K. Ohyama, "Comparison of switching losses of matrix converters for commutation methods," in *2014 16th European Conference on Power Electronics and Applications*, DOI 10.1109/EPE.2014.6910995, pp. 1–10, Aug. 2014.

[7] Y. Guo, Y. Guo, W. Deng, J. Zhu, and F. Blaabjerg, "An improved 4-step commutation method application for matrix converter," in *2014 17th International Conference on Electrical Machines and Systems (ICEMS)*, DOI 10.1109/ICEMS.2014.7014112, pp. 3590–3593, Oct. 2014.

[8] H. M. Nguyen, H.-H. Lee, and T.-W. Chun, "Input power factor compensation algorithms using a new direct-svm method for matrix converter," *IEEE Trans. Ind. Electron.*, vol. 58, DOI 10.1109/TIE.2010.2044736, no. 1, pp. 232–243, Jan. 2011.

[9] M. Apap, J. Clare, P. Wheeler, and K. Bradley, "Analysis and comparison of ac-ac matrix converter control strategies," *IEEE 34th Annual Conference on Power Electronics Specialist*, DOI 10.1109/PESC.2003.1216774, pp. 1287–1292, Jun. 2003.

[10] W. Xiong, Y. Sun, J. Lin, M. Su, H. Dan, M. Rivera, and J. M. Guerrero, "A cost-effective and low-complexity predictive control for matrix converters under unbalanced grid voltage conditions," *IEEE Access*, vol. 7, DOI 10.1109/ACCESS.2019.2908446, pp. 43 895–43 905, 2019.

[11] Imdadullah, S. M. Amrr, M. S. Jamil Asghar, I. Ashraf, and M. Meraj, "A comprehensive review of power flow controllers in interconnected power system networks," *IEEE Access*, vol. 8, DOI 10.1109/ACCESS.2020.2968461, pp. 18 036–18 063, 2020.

[12] J. Monteiro, J. F. Silva, S. F. Pinto, and J. Palma, "Matrix converter-based unified power-flow controllers: Advanced direct power control method," *IEEE Transactions on Power Delivery*, vol. 26, DOI 10.1109/TPWRD.2010.2055897, no. 1, pp. 420–430, 2011.

[13] J. Monteiro, J. F. Silva, S. F. Pinto, and J. Palma, "Linear and sliding-mode control design for matrix converter-based unified power flow controllers," *IEEE Transactions on Power Electronics*, vol. 29, DOI 10.1109/TPEL.2013.2282256, no. 7, pp. 3357–3367, 2014.

[14] M. B. Shadmand, M. Mosa, R. S. Balog, and H. Abu-Rub, "Model predictive control of a capacitorless matrix converter-based statcom," *IEEE Journal of Emerging and Selected Topics in Power Electronics*, vol. 5, DOI 10.1109/JESTPE.2016.2638883, no. 2, pp. 796–808, 2017.

[15] P. Szczesniak and J. Kaniewski, "Hybrid transformer with matrix converter," *IEEE Transactions on Power Delivery*, vol. 31, DOI 10.1109/TPWRD.2015.2493508, no. 3, pp. 1388–1396, 2016.

[16] P. Szczesniak, G. Tadra, J. Kaniewski, and Z. Fedyczak, "Model predictive control algorithm of ac voltage stabilizer based on hybrid transformer with a matrix converter," *Electric Power Systems Research*, vol. 170, DOI https://doi.org/10.1016/j.epsr.2019.01.024, pp. 222–228, 2019. [Online]. Available: https://www.sciencedirect.com/science/article/pii/S0378779619300367

[17] P. Szczesniak and J. Kaniewski, "Power electronics converters without dc energy storage in the future electrical power network," *Electric Power Systems Research*, vol. 129, DOI https://doi.org/10.1016/j.epsr.2015.08.006, pp. 194–207, 2015. [Online]. Available: https://www.sciencedirect.com/science/article/pii/S0378779615002436

[18] S. M. Ahmed, A. Iqbal, and H. Abu-Rub, "Generalized duty-ratio-based pulsewidth modulation technique for a three-to-k phase matrix converter," *IEEE Trans. Ind. Electron.*, vol. 58, DOI 10.1109/TIE.2010.2098373, no. 9, pp. 3925–3937, Sep. 2011.

[19] M. Ali, A. Iqbal, M. R. Khan, M. Ayyub, and M. A. Anees, "Generalized theory and analysis of scalar modulation techniques for a $m \times n$ matrix converter," *IEEE Transactions on Power Electronics*, vol. 32, DOI 10.1109/TPEL.2016.2600034, no. 6, pp. 4864–4877, Jun. 2017.

[20] A. Alesina and M. G. B. Venturini, "Analysis and design of optimum-amplitude nine-switch direct ac-ac converters," *IEEE Transactions on Power Electronics*, vol. 4, no. 1, pp. 101–112, 1989.

[21] J. Zhang, L. Li, and D. G. Dorrell, "Control and applications of direct matrix converters: A review," *Chinese Journal of Electrical Engineering*, vol. 4, DOI 10.23919/CJEE.2018.8409346, no. 2, pp. 18–27, 2018.

[22] J. Igney and M. Braun, "A new matrix converter modulation strategy maximizing the control range," in *2004 IEEE 35th Annual Power Electronics Specialists Conference (IEEE Cat. No.04CH37551)*, vol. 4, DOI 10.1109/PESC.2004.1355290, pp. 2875–2880 Vol.4, 2004.

[23] X. Li, M. Su, Y. Sun, H. Dan, and W. Xiong, "Modulation strategy based on mathematical construction for matrix converter extending the input reactive power range," *IEEE Transactions on Power Electronics*, vol. 29, DOI 10.1109/TPEL.2013.2256929, no. 2, pp. 654–664, 2014.

[24] L. Zarri, M. Mengoni, A. Tani, and J. O. Ojo, "Range of the linear modulation in matrix converters," *IEEE Transactions on Power Electronics*, vol. 29, DOI 10.1109/TPEL.2013.2274285, no. 6, pp. 3166–3178, 2014.

[25] F. Schafmeister and J. W. Kolar, "Novel hybrid modulation schemes significantly extending the reactive power control range of all matrix converter topologies with low computational effort," *IEEE Transactions on Industrial Electronics*, vol. 59, DOI 10.1109/TIE.2011.2158045, no. 1, pp. 194–210, 2012.

[26] L. Qiu, Y. Li, X. Huang, L. Wu, and Y. Fang, "Modulation technique for a 3x5 matrix converter achieving a maximum input reactive power range based on load information," *IEEE Transactions on Power Electronics*, vol. 36, DOI 10.1109/TPEL.2021.3059405, no. 9, pp. 10 409–10 419, 2021.

[27] P. Szczepankowski, P. Wheeler, and T. Bajdecki, "Application of analytic signal and smooth interpolation in pulsewidth modulation for conventional matrix converters," *IEEE Transactions on Industrial Electronics*, vol. 67, DOI 10.1109/TIE.2019.2956391, no. 12, pp. 10 011–10 023, 2020.

[28] P. Szczepankowski, T. Bajdecki, and R. Strzelecki, "Direct modulation for conventional matrix converters using analytical signals and barycentric coordinates," *IEEE Access*, vol. 8, pp. 22 592–22 616, 2020.

[29] P. Szczepankowski and J. Nieznanski, "Application of barycentric coordinates in space vector pwm computations," *IEEE Access*, vol. 7, DOI 10.1109/ACCESS.2019.2914854, pp. 91 499–91 508, 2019.

[30] P. Szczepankowski, W. Sleszynski, and T. Bajdecki, "A direct modulation for matrix converters based on the onecycle atomic operation developed in verilog hdl." *IEEE Transactions on Industrial Electronics*, DOI 10.1109/TIE.2021.3076703, pp. 1–1, 2021.

[31] E. Levi, "Multi-phase machines for variable speed applications," *IEEE Trans. Ind. Electron.*, vol. 55, DOI 10.1109/TIE.2008.918488, no. 5, pp. 1893–1909, May. 2008.

[32] E. Levi, R. Bojoi, F. Profumo, H. Toliyat, and S. Williamson, "Multi-phase induction motor drives-a technology status review," *IET Elect. Power Appl.*, vol. 1, DOI 10.1049/iet-epa:20060342, no. 4, pp. 489–516, Jul. 2007.

Pawel Szczepankowski (M'18) received his D.Sc. in 2020 from Gdansk University of Technology, Poland. His research interests include design, control, diagnostics, modelling and simulation of power electronic converters, including multilevel, matrix and modular topologies. He deals with designing and programming microprocessor control systems with DSP processors and FPGA devices.